Review

Output of a tidal farm in yawed flow and varying turbulence using GAD-CFD

Charles E. Badoe, Xiaorong Li, Alison J. Williams [*], Ian Masters

Energy and Environment Research Group, Zienkiewicz Centre for Computational Engineering, College of Engineering, Bay Campus, Swansea University, SA1 8EN, Wales, UK

ABSTRACT

Tidal stream turbine arrays will be subject to a range of flow conditions throughout the tidal cycle and it is important for developers to have an understanding of the impact of these on array performance when planning site design. A generalised actuator disk-computational fluid dynamics (GAD-CFD) model is used to conduct simulations on a three and fourteen turbine array arranged in two different configurations. Firstly, simulations of both arrays are conducted in straight flow conditions to understand the hydrodynamics around devices and evaluate their performance. Performance predictions for the three turbine array in straight flow conditions are in close agreement with previous studies. In the fourteen turbine array, wake recovery to free-stream conditions was better in the modified formation compared to the regular formation and the total power output was increased by over 10%. The influence of yaw angle and upstream TI (turbulence intensity) on both array performance was also studied. Strong sensitivity of overall farm power and thrust was found to exist in small variations in yaw angle. However, the overall wake structures were similar irrespective of the yaw angle.

Finally, simulations of different turbulence intensities showed rapid decay shortly downstream of the inlet. In all arrays, turbulence intensity had little effect on the thrust and power of the upstream set of devices for the considered TI range but greatly influenced the individual downstream devices.

1. Introduction

Tidal stream power generation is currently undergoing rapid progressing as a reliable form of renewable energy due to the predictability of tidal periods and magnitudes (Bahaj et al., 2013). A number of sites across the world are being identified and tidal current turbines installed in small arrays to generate and export electricity to local networks (The Crown Estate, 2018). However, a lot of the sites that have been identified for installation of these devices exhibits some degree of misalignment in incident flow, more especially in nearshore environments where bathymetric and seabed frictional effects are significant. Misalignment in incident flow or yawed inflow may also occur due to turbine support structures and the presence of upstream bluff bodies (Piano et al., 2017). When a tidal current turbine experiences misalignment in incident flow or yawed inflow, the flow of water is no longer aligned with the turbine and crossflow is developed across the turbine plane. This will alter the turbine's thrust and power as well as changing the effective direction of the turbine race. The net sideforce due to the turbine will vary more than during straight flow conditions. Wake behaviour will also vary compared to straight flow conditions. Yaw misalignment effects therefore play an important role and quantification of a turbine's performance and wake details under

such condition is essential for the design layout of a tidal farm for maximising the power output (Adaramola and Krogstad, 2011).

A number of experimental studies have been conducted to improve understanding of yawed inflow influence on tidal turbines. For example, Galloway et al. (2011) studied the power and thrust performance of a scaled tidal current turbine operating at yaw and in waves in a tow tank. The authors observed that less power and rotor thrust was captured by the turbine and resulted in reduced performance as yaw angle increased. Galloway et al. (2014) followed on his earlier work by conducting experiments to study the cyclic loading and fatigue effects due to dynamic yaw on a rotor caused by wave–current interaction. They found that yaw angles below 7.5 degrees had negligible effect on the rotor. Maganga et al. (2009) conducted experimental studies to quantify the effects of flow characteristics (yaw and velocity gradient) on the performance and loading on a tidal turbine. The authors observed that the turbine's performance was sensitive to the quality of the incoming flow and a misalignment of a fixed turbine can cause significant losses. Zhang et al. (2023) studied the effects of a turbine operating under varying yaw conditions. Their results showed that increasing yaw angle results in a decrease in the turbine's streamwise force and an increase in spanwise force. Velocity distributions also showed that the

---

wake deflection and velocity deficit recovery rate increased at a rate proportional to the yaw angle. Modali et al. (2018) studied turbine performance and wake deflection within ± 15° yawed conditions and showed that when an upstream turbine is yawed, the downstream turbine can extract more than 50% higher energy in a staggered layout than in an aligned layout. All of the above experimental work provides an opportunity to evaluate the performance of the tidal devices in a relatively low-cost, controlled laboratory environment, which can also be used to complement and validate numerical models.

Computational fluid dynamics (CFD) has also been used, through a number of approaches to study the performance and wake details of tidal devices under yawed inflow conditions. Each approach has advantages and disadvantages, with the main balance being a trade off between detailed simulation of the physics and the computational time and resources required to achieve a result. At the smallest and most detailed scale, fully resolved tidal current turbine geometry models have been used to provide insight into the development of the wake structures downstream of a device (Tian et al., 2016; Tongchitpakdee et al., 2005; O'Doherty et al., 2009a). Turbulence was resolved using either Reynolds-averaged Navier–Stokes (O'Doherty et al., 2009b) or Large Eddy Simulations (McNaughton et al., 2013). However, these approaches require small time steps due to restrictions imposed by explicitly solving the turbine flow, thus placing a high demand on computation. As such, they are not feasible when considering simulation of large arrays of full-scale turbines. In addition, high computational cost restricts simulation of a wide range of incident environmental conditions, which are known, for tidal energy sites, to be highly variable resulting from complex combinations of waves, currents and turbulence. Computations of this nature are often performed using momentum source models.

Momentum source models are able to compute the force distributions along the rotor blades, and determine the overall performance of a turbine. Significantly lower computational requirements and fast processing time can be exploited where many analyses are required. Howland et al. (2016) used an actuator disk model, to investigate wake deflections of a turbine under yawed conditions. Their findings suggest that when a turbine is yawed for the benefit of downstream turbines, the curled shape of the wake and its asymmetry must be taken into account since this affects how much of it interacts with the downstream turbines. Baratchi et al. (2017) used an actuator line method to study the performance and wake of the tidal turbine in both straight and yawed flow. Their results showed good agreement with the measurements published in Bahaj et al. (2007). Gao et al. (2021) coupled an actuator line method to large eddy simulations to study the wake characteristics of a turbine under various yaw conditions. They showed that wake skew exacerbates the instability of the tip vortex and causes the wake region to narrow. At lower yaw angles, nacelle vortex radially diffuses and blends with the tip vortex in the far wake whilst at higher yaw angles, the nacelle vortex intercepts the tip vortex in the near wake due to the different spatial distribution of thrust.

Despite the valuable insight from these experimental and numerical studies, there is still a gap in the performance and wake details of tidal current turbines in arrays as most of these studies were carried out for either one or two turbines. The wake generated by for example, the front set of turbines in a large tidal turbine farm can cause disturbance to the rear set of turbines in straight flow conditions and significantly increase in angled incoming flow conditions (Schulz et al., 2017). Very large computational resources are also needed to capture and understand such flow detail. There are also open questions about the wake details, for example, its propagation and extent of recovery in yaw conditions.

One particular area of research which has gained momentum in recent years and has been used to compute multiple tidal current turbines in arrays is the Blade Element Theory combined with Computational Fluid Dynamics simulation techniques (BEM-CFD) (Malki et al., 2013; Turnock et al., 2011). The BEM-CFD models utilises radially varying set of turbine blade characteristics, distributed uniformly in an axial direction. Hence, computational cells at the same radius from the turbine centre have the same properties, however, as the flow varies from cell to cell, the resultant forces on the fluid also vary. The model can allow the local environment to be simulated providing a comprehensive study of a tidal farm and wake at a reduced computational cost (Olczak et al., 2014). The application of tip loss corrections and downwash pertinent to a CFD type model representation takes the BEM-CFD approach further. This extension, the Generalised Actuator Disk (GAD-CFD), has provided confidence when applied to laboratory scale flume studies (Edmunds et al., 2017a). The GAD-CFD model includes new improved features such as a more concise downwash distribution computation, variation of foil section, application of tip radius correction, variation of lift/drag curves with Reynolds number and surface roughness. The use of analytical methods to successfully and effectively predict the distribution of lift towards the tip of finite wing, have been demonstrated to produce reasonable estimates of thrust and power (Edmunds et al., 2020). Allowing for the variation of foil section shape within the model adds to the refinements including the distribution of forces along the foils. This helps produce slightly better characteristics closer to the rotor hub, and also improved prediction in the stall region of the TSR range. The benefit of the GAD-CFD approach, with respect to computational cost, is unequivocal and allows us to move into the realms of array interaction modelling and site design at a more reasonable level of cost (Badoe et al., 2022a).

In this work, the effectiveness of the GAD-CFD approach in accurately capturing fluid-machine interaction for multiple tidal energy converters subject to yawed flow conditions is assessed. The GAD-CFD model is first used to simulate a three-turbine array in straight flow, β = 0°, and the results compared with physical tank-testing conducted at the FloWave facility (Noble et al., 2020, 2015; Sutherland et al., 2017). Additional simulations are then conducted at yawed angles, β = 4° and 8° to study yaw effects. A second simulation is conducted to further assess the performance of the approach, in terms of the capacity to model multiple full-scale turbines in more varied configuration. The current work extends our previous work in Malki et al. (2014) and Edmunds et al. (2017b) to provide a better understanding of the influence of rotor spacing on the hydrodynamics around devices, leading to optimised performance for large arrays.

Finally, as turbulence intensity also impacts the fluid-machine interactions associated with the turbine energy production, simulations under straight flow conditions with varying incoming turbulence intensities are also performed and analysed. This demonstrates how the GAD-CFD tool can be useful to developers in real projects.

2. Numerical methodology

2.1. Governing equations

The OpenFOAM toolbox (Weller et al., 1998) is utilised for the model implementation. The OpenFOAM toolkit provides a range of standard solvers which can be modified for use with the additional turbine physics. The additional GAD source terms are implemented in the steady state Reynolds Averaged Navier Stokes (RANS) "simpleFoam" solver. A more detailed description of the GAD-CFD model including the extended downwash distribution method and coupling strategy is presented in Edmunds et al. (2020) and Badoe et al. (2022a). Within the assumption of an incompressible fluid, the set of equations may be written in the form:

$$\frac{\partial \overline{U}_i}{\partial x_i} = 0 \tag{1}$$

$$\frac{\partial \overline{U}_i}{\partial t} + \frac{\partial \overline{U_i U_j}}{\partial x_j} = -\frac{1}{\rho}\frac{\partial \overline{P}}{\partial x_i} + \frac{\partial}{\partial x_j}\left(\nu\left(\frac{\partial \overline{U}_i}{\partial x_j} + \frac{\partial \overline{U}_j}{\partial x_i} \right) \right) - \frac{\partial \overline{u'_i u'_j}}{\partial x_j} + f_i, \tag{2}$$

Table 1
Three-turbine array dimensions.

Parameter	Dimension [m]
Rotor diameter	1.2 (1D)
Nacelle length	1.03
Nacelle diameter, hub to tower	0.12
Nacelle diameter, beyond tower	0.16
Hub height	1.0 (0.83D)
Tower diameter	0.102
Distance from rotor plane to tower axis	0.486 (0.4D)

where x_i represents the Cartesian coordinates (X, Y, Z), U_i is the Cartesian mean velocity components ($\overline{U}_x, \overline{U}_y, \overline{U}_z$) and f_i includes an additional source representing the disc rotor characteristics. The Reynolds stress is $\overline{u'_i u'_j}$ and must be modelled to close the governing equations by employing an appropriate turbulence model.

The k-ϵ RNG turbulence model (Payne et al., 2017) has been used for this work. In this model two equations are solved; k represents the energy contained within the turbulent fluctuations, and ϵ represents the dissipation rate of this energy. The equations for the transport of these variables are similar in form to the momentum equations. The model has been credible when applied to flows involving large rotating downstream wakes (Badoe et al., 2022b, 2021) which is one of the key aspects of the present application. However, the models are also known to sometimes over-predict wake lengths, mainly due to the turbulence dissipation turbulent kinetic energy which can influence the loadings on downstream turbines (Ebdon et al., 2016).

3. Case study 1: Three turbine array turbine

3.1. Turbine arrangements

Using the GAD-CFD model, a three turbine array as shown in Fig. 1 is simulated. The hubs of these two upstream turbines are 1 D upstream and 1.5 D either side of the primary turbine, giving a transverse separation of 3 D. This configuration was shown in Badoe et al. (2022a) to accelerate the flow experienced by the rear turbine and improve its performance. Additionally, the front row being only 1 D in front of the primary turbine, means that the rear turbine is not in the wake of the front two turbines. The turbines are generic bed-mounted, fixed-pitch, three-bladed horizontal axis design. The turbine models are 1:15 scale, corresponding to an 18 m diameter prototype. Table 1 summarises the principal dimensions of the turbines. Turbine rotational speed is set to be the same for all turbines, so that they have a tip speed ratio (TSR), of 7.0 relative to the inlet velocity. The turbine geometries were based on the NACA63812 and 63815 aerofoil sections and a separate CFD study was conducted to determine a set of lift and drag curves at a range of Reynolds numbers and turbulence levels required for these sections to use for this study. The chord-length Reynolds numbers vary between 0.5×10^5 (root) and 2.5×10^5 (tip). Physical tank testing experiments have been conducted in straight flow conditions, $\beta = 0°$. Full details of the experiments can be found in Noble et al. (2020).

3.2. Domains and boundary condition

The entire flow field was considered as a result of asymmetry of the flow induced by the oblique motion and rotation induced by the turbines. Turbine yaw angle was achieved by keeping the inflow/domain fixed and rotating the turbines as per the required yaw angle. This technique was automated by employing a script which, when called upon, allows rotation of the turbines within the domain to the required yaw angle. The domain size represents the FloWave tank dimensions, see also Fig. 2. The nominal inflow velocity of 0.8 m/s was set at the inlet. This corresponds to a full-scale flow speed of 3.1 m/s. Flow rates are set at the inlet vents. In the physical tank testing experiments, the turbulence intensity at the turbine location was recorded to be
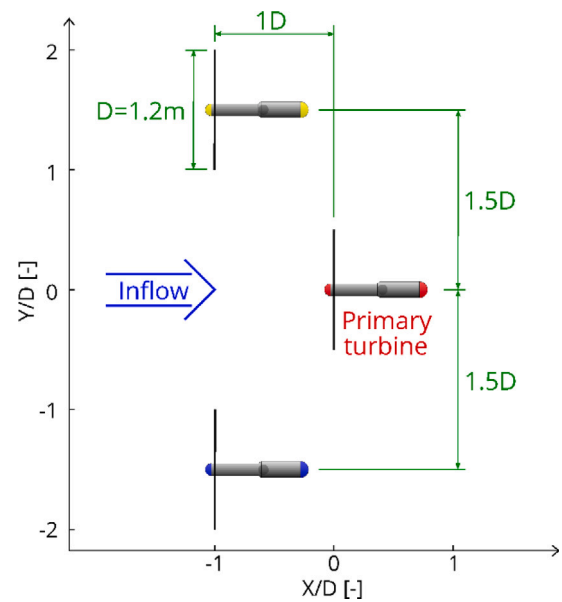

Fig. 1. Schematics of the three-turbine array layout (not to scale). Turbine 1 denotes the primary turbine, Turbines 2 and 3 denote the right and left upstream turbines in the inflow direction respectively.

Table 2
Computational parameters.

Parameter	Settings
Computing	Astute Linux Cluster[a]
Mesh type	Unstructured hexahedral
Turbulence model	k-ϵ RNG
Pressure velocity coupling	SIMPLE
y^+ average (nacelle)	30
Grad (U) scheme	Gauss linear
Convergence criteria	RMS residual $< 10^{-3}$

Note: Run type and Parallel run (14 partitions run on 2 × dual core nodes).
[a] http://enhpc-wiki.swan.ac.uk.

Table 3
Simulation flow conditions.

Yaw, β (°)	Turbulence intensity, TI (%)
0	15
0	25
0	30
4	15
8	15

approximately 7% for the flow velocity used (Noble et al., 2020). The tank walls are set to zero velocity and wall functions used for k, ϵ, and *nut*. The top of the domain is set to a full slip condition representing the open fluid surface. The initial conditions are mapped to the boundary conditions in all but velocity. The initial velocity condition is set to zero. The kinematic viscosity ν of this problem is set to $1.6667e^{-6}$ m² s⁻¹. No roughness parameter was added and the bottom boundary assumed a smooth wall. Table 2 summarises the computational parameters adopted for this study. Five flow configurations have been investigated, as illustrated in Table 3.

3.3. Grid generation

The grids were created utilising both "blockMesh" and "snappyHexMesh" in OpenFOAM. First, an initial structured hexahedral background mesh consisting of a block topology structure was generated which captures the domain extents of thirty metres square and four
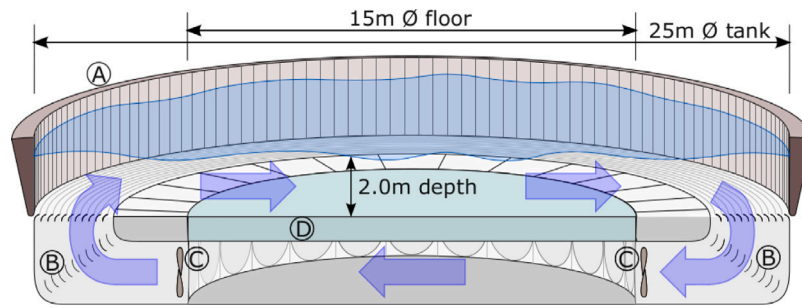
Fig. 2. Sectional schematic of FloWave basin showing: (A) wavemaker paddles around circumference; (B) turning vanes and flow conditioning filters; (C) current drive impeller units; (D) buoyant raisable floor (15 m∅) below test area (Noble et al., 2015).

Table 4
Table of initial mesh subdivisions for the set of meshes studied. The total cell count is post refinement using the snappyHexMesh utility.

Mesh	Subdivisions	Total no of cells
G1	100 × 100 × 30	95 686
G2	200 × 200 × 60	766 968
G3	300 × 300 × 90	2 590 032
G4	400 × 400 × 120	6 146 016
G5	500 × 500 × 150	11 998 116
G6	600 × 600 × 180	20 740 456

metres deep. The domain is then subdivided using divisions defined in Table 4. With reference to Fig. 3, refinement of the mesh around the turbines and wake region is achieved using the "snappyHexMesh" utility. The wake region is defined as a cylinder 0.7 metre radius, extending from the rotor to 9 metres downstream, i.e. to the domain outflow. The refinement level in this region is specified as level 2, the base cell/mesh is subdivided twice in this region (Note 2 in Fig. 3). The rotor assembly and bladebox is set with a refinement level of 5, i.e. Note 5 in Fig. 3. The region around the rotor assembly (Note 3 in Fig. 3) is set at level 3 up to 0.1 metres from the assembly. A reasonable level of detail of the nacelle and support is included in the model as shown in Fig. 3.

For the mesh independence study an examination of the coefficients of power, C_P and coefficients of thrust C_T is performed for a single rotor in straight inflow conditions, $\beta = 0°$. It can be seen in Fig. 4 that the coefficients tend to not change significantly after mesh density G4. Based on the study, mesh G4 (see Table 4), representing a reasonable compromise in accuracy and computational cost, was chosen to perform the remaining studies.

3.4. Results

3.4.1. Performance at different yaw angles

The tidal stream configuration performances at yaw was quantified by comparing the yaw results with the straight flow cases. Two yawed inflow cases were considered, i.e, $\beta = 4°$ and $8°$. As already pointed out, the turbines have been fully tested experimentally at $\beta = 0°$ and the results have been included for comparison purpose. Fig. 5 demonstrates the performance of all turbines in the array model in terms of C_P and C_T at TSR = 7. Compared to the experiment, GAD-CFD predicts the thrust and power of the primary rotor (Turbine 1) within 3.5% and 9.5% respectively for $\beta = 0°$. The GAD-CFD model only reports thrust acting directly on the rotor, thus a correction needs to be calculated considering the fluid drag acting on the assembly. This issue has been examined in Edmunds et al. (2017b) and demonstrated good correlation for the combined results of thrust. RANS based models including the GAD-CFD model are known to under-predict how much of the energy exerted on the turbine will be converted into rotation on the blades and hence useful power. This has also been reported by Ebdon et al. (2016) and Batten et al. (2013). C_P under prediction may also
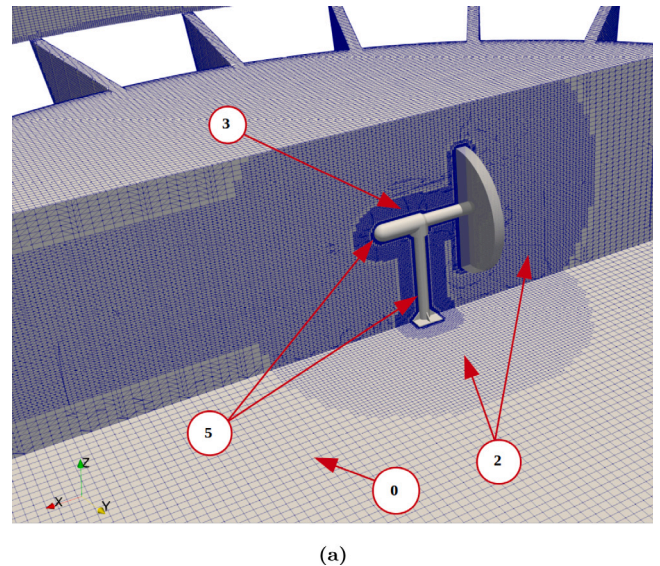

(a)

Fig. 3. Mesh topology generated using a combination of "blockMesh" and "snappyHexMesh" utilities. Note 0 shows the outer/base distribution of cells, while Note 2 shows the level 2 refinements made in the wake region. Note 3 identifies the assembly area refinement, and Note 5 identifies the level 5 assembly region.

be attributed to variations in local flow directions at the blades and numerical rounding in the model. With this in mind the thrust and power characteristics correlate well and show a similar trend to the observations of the experimental results (see also Fig. 4). Compared to the other turbines, the primary rotor (Turbine 1) also produces the most power. This is because it benefits from the accelerated approaching flow from the two upstream turbines (Turbines 2 and 3). Having higher velocities approaching the turbine can result in an increase in the extractable power.

The trend in both power and thrust curves for the different angles of yaw are also identical. C_P and C_T decreases as yaw angle increases. This is because as the incoming flow is no longer aligned to the turbine blades, a crossflow is developed across the turbine plane and as the yaw angle increases, the axial component of the velocity reduces, leading to less lift and hence torque. Another problem regarding the reduction in C_P with increase in yaw angle may be attributed to the separation of the nacelle and the flow in the vicinity of the rotor. As yaw increases, the separation at the nose of the nacelle becomes greater. This causes the flow in the vicinity of the turbine to be more turbulent. Lastly, the blockage by the turbines to the flow can be felt upstream, leading to greater deficit in the wake region and a corresponding decrease in power. The overall power was reduced by 3.0% and 5.0% for $\beta = 4°$ and $8°$ respectively compared to the $\beta = 0°$ case. Additionally, the thrust also reduced by 2.0% to 4.0% for $\beta = 4°$ and $8°$ respectively compared to the $\beta = 0°$ case. Fig. 6 shows the differences in the wake
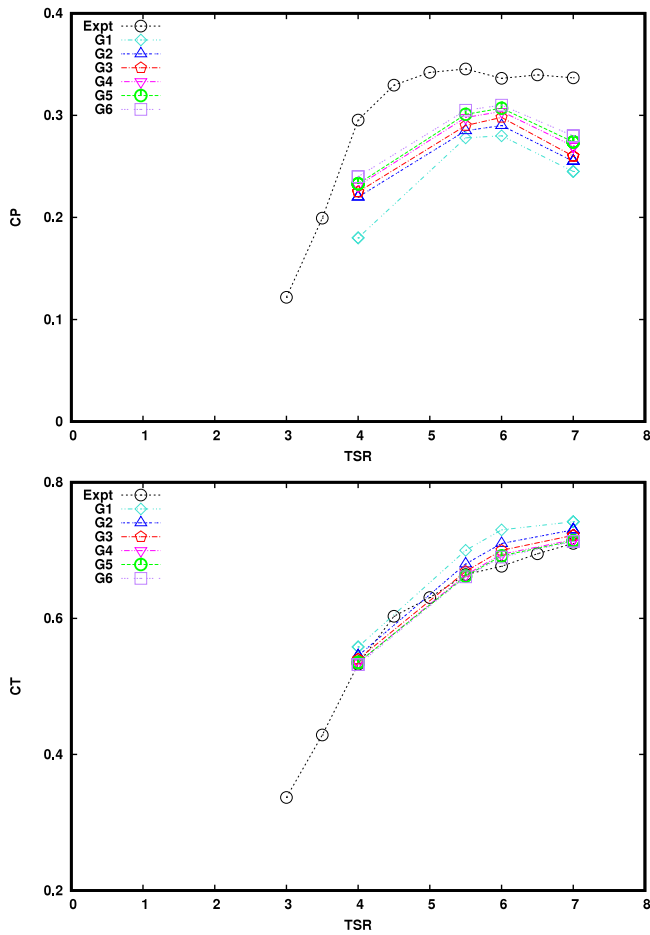
Fig. 4. Coefficients of power, C_P (top) and thrust, C_T (bottom) plotted against mesh number from coarsest (G1) to finest (G6).

Fig. 5. Comparison of coefficient of power C_P (bottom) and coefficient of thrust C_T (bottom) at different yaw angles, TI = 15%, TSR = 7.

3.4.2. Performance at different upstream turbulence intensities, $TI's$

Interaction of turbulence with tidal turbines is important if accurate fatigue predictions are to be made and turbine reliability optimised. To consider the effects of turbulence intensity, the three turbine array is compared with three inlet turbulence intensities, $TI's$ of 15%, 25% and 30% at $\beta = 0°$. Fig. 8 shows turbulence intensity decay variation as they progress downstream to the turbines. The two upstream turbines (Turbines 2 and 3) are located at $x = -1.2$ m whilst the located of the primary turbine (Turbine 1) is at $x = 0$ m. The plot shows a rapid decay shortly downstream of the inlet as well as close to the turbines. At inlet $TI's$ of 15%, 25% and 30%, only TI of 7%, 10% and 10.5% respectively were realised at the locations of Turbines 2 and 3, corresponding to a 53%, 60% and 65.5% drop in turbulence intensity. As seen in Fig. 8, the results are consistent with the experimental measurements.

Fig. 9 shows that increasing the turbulence intensity, TI has little effect on the mean C_P and C_T for the $TI's$ evaluated in this analysis, with less than 3.5% difference. Previous studies (Modali et al., 2018; Tian et al., 2016) have also shown that the mean C_P and C_T are only slightly dependent on the turbulence intensity at TSR values of $1 \leq TSR \leq 10$. The results show an increase of 2.0% in power production when inlet TI is increased from 15% to 25% and a further 1.2% from 25% to 30%.

Fig. 10 shows the wake velocity for the investigated $TI's$. The results show similar near wake features, however there are visible differences in the far wake features. Concerning the profiles of velocities calculated downstream of the arrays in Fig. 11, it can be seen that, large differences exist between the different turbulence rates (seen more clearly at $x/D > 2$). The maximum deficit was observed for the lowest turbulence rate in all locations with the peak occurring at $x/D = 2.5$. The results suggest that turbulence intensity has little influence on the near wake of the array, but helps to recover the axial velocity in the wake. This finding is consistent with previous research (Tian et al., 2016).

4. Case study 2: Multiple full-scale turbines in varied configuration

4.1. Turbine arrangements

A fourteen-turbine array with two different arrangements was also simulated. The first is a 4 row arrangement whereby the lateral and longitudinal spacing are 3.0 diameters and 10.0 diameters respectively (regular formation), see top image in Fig. 12. These are arbitrary

structure for the various yaw angles. There is a slight increase in the skewness in the wake as well as a slight decrease in the recovery distance as yaw angle increases. This has also been reported by Tian et al. (2016) at a similar TSR value. As the wake propagates downstream, it also deviates slightly from the direction of yaw.

Line samples of the velocities were taken downstream (Fig. 7) of the primary rotor to capture the fluid characteristics exiting the array for the different yaw angles. The samples were taken at six x/D locations. Results for the $\beta = 0°$ case demonstrates that the wakefield generated by the array compares well with experimental values. For yaw influence, the profiles are different for turbines 2 and 3 compared to the primary turbine in the near wake, i.e $x/D \leq 2.5$. In turbines 2 and 3, there is a shift in the profiles compared to the $\beta = 0°$ profile. However, for the primary turbine (or turbine 1), the profiles show similar behaviour. When tidal arrays experience misalignment in flow conditions, the net sideforce will vary more than during straight ahead conditions resulting in a decrease in effective inflow angle, especially to a downstream turbine. At the same time an upstream turbine can block and straighten the flow to the downstream turbine, leading to a recovery in effective inflow angle to the downstream turbine. It is possible that the blockage by the two upstream turbines may have contributed to the behaviour of the primary turbine profile. Interestingly, for the two upstream turbines, the plots also show that $\beta = 0°$ has the largest velocity deficit for turbine 3 whereas it has the smallest velocity deficit for turbine 2.

At $x/D > 2.5$ (Fig. 7d–f, see also Fig. 6), the peak velocity deficits in the combined or individual wakes is higher for $\beta = 0°$ compared to the yaw cases. This may be as a results of the higher turbulence levels in the yawed flow cases.
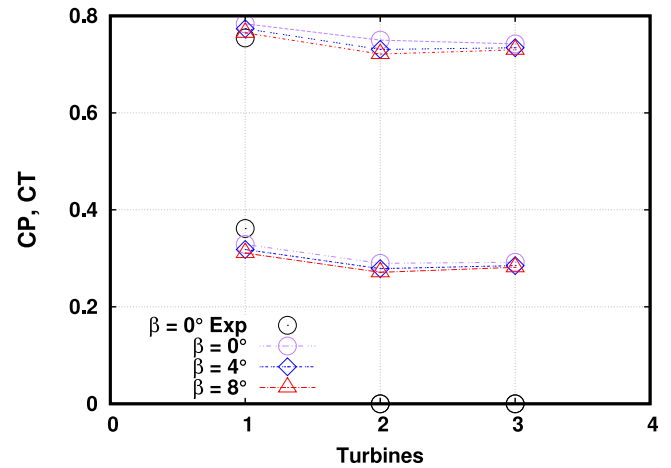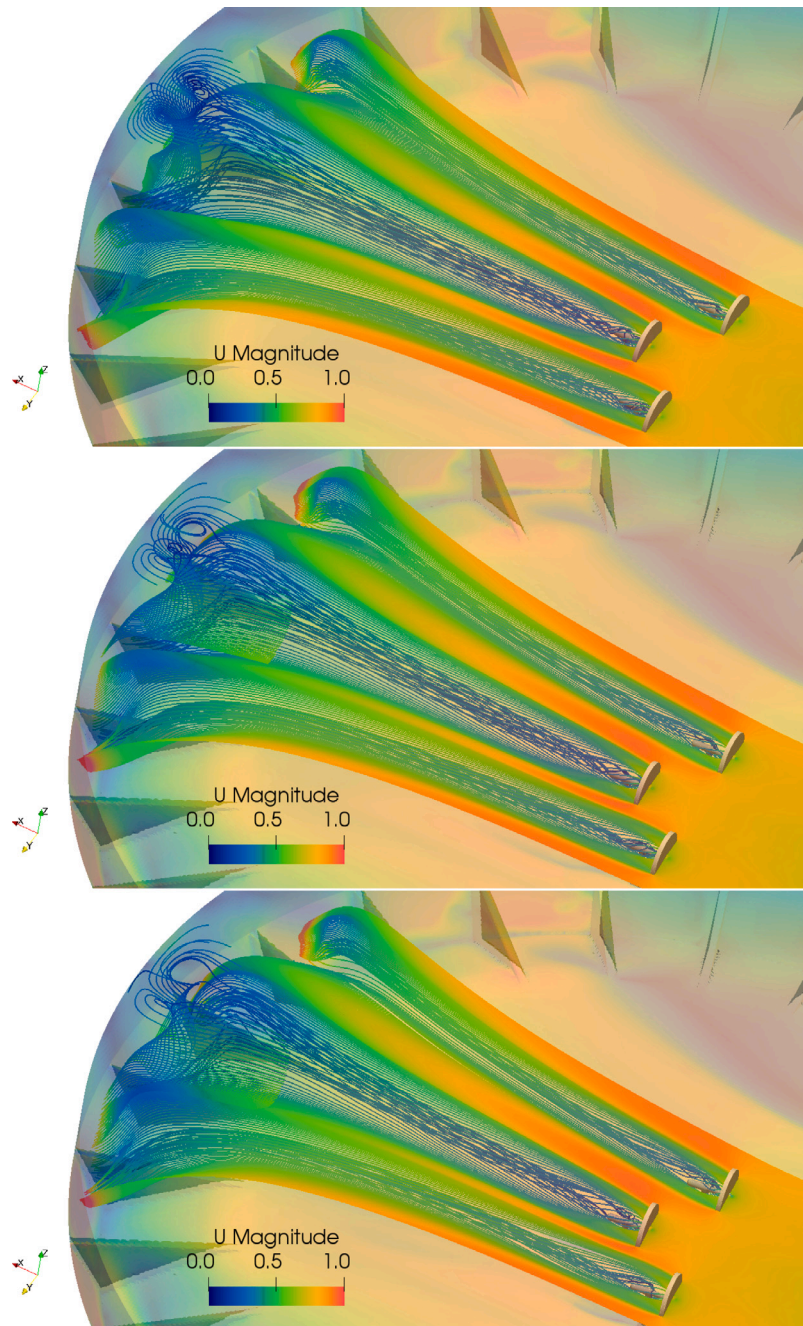
Fig. 6. Wake velocity for the three turbine array at different yaw angles. Top to bottom: $\beta = 0°$, $4°$, $8°$. Note: Increase in yaw angle is in a clockwise direction.

values which have been chosen to reproduce reasonable turbine spacing that may be implemented in a real situation. The second arrangement presented in Fig. 12, bottom image shows a different arrangement in which the lateral spacing between devices is increased to 4.0 diameters to maximise the flow acceleration between them (modified formation). The second and third rows have been moved so that they are one diameter away from the first and fourth rows such that the distance between the second and third row is 38.0 diameters. This serves two purposes, firstly the second and fourth rows will benefit from flow acceleration between upstream turbines to a greater extent. Secondly, such an arrangement will also facilitate a greater level of flow recovery before the flow interacts with the third and fourth rows. The turbines are fixed pitch variable speed, running at an optimal TSR of 3.0 based on the inlet velocity. Turbine rotational speed was set to be the same for the turbines, so that they have TSR of 3.0 relative to the inlet velocity.

The turbines have a diameter of 10 m which is a reasonable representation of the scale of turbines likely to be deployed in nearshore environments. The chord length and chord twist angle characteristics of the blade are presented in Fig. 13. The rotor geometry, and lift/drag characteristics, are also taken from Malki et al. (2014). The NACA 4424 lift and drag curves are taken from Abbott and Von Doenhoff (1959) with chord-length Reynolds numbers varying between 0.2×10^6 (root) and 1.0×10^6 (tip).

4.2. Domain and boundary conditions

The inflow and outflow plane were located 30 D upstream of the front turbines and 60 D downstream of the rear turbines respectively. A cuboid computational domain is employed. The domain is 1200 metres in length (x-axis). The domain depth is 30 metres (z-axis), while the
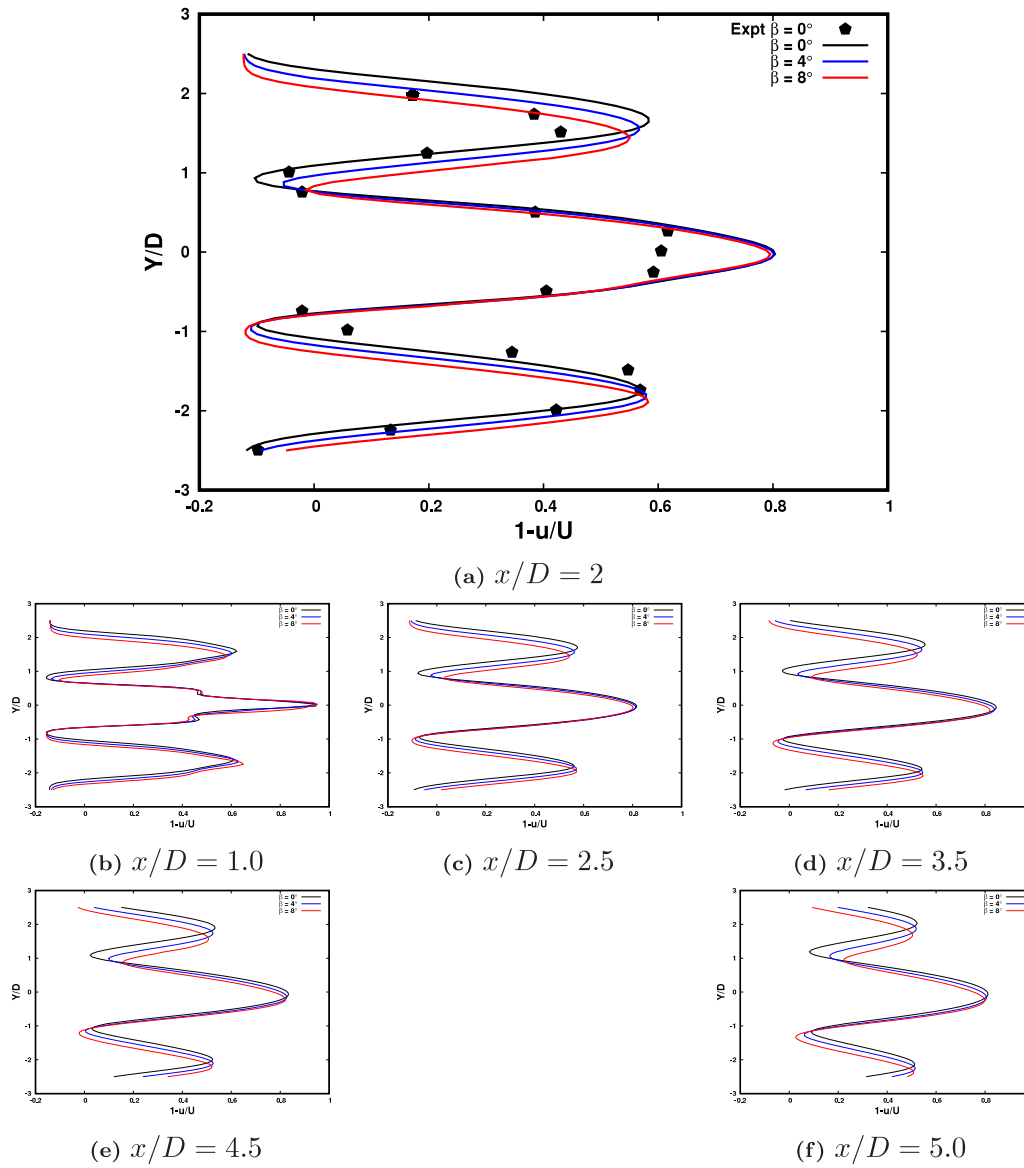
(a) $x/D = 2$

(b) $x/D = 1.0$

(c) $x/D = 2.5$

(d) $x/D = 3.5$

(e) $x/D = 4.5$

(f) $x/D = 5.0$

Fig. 7. Transverse profiles of normalised downstream axial velocities at three different yaw angles, $\beta = 0°$, $4°$, $8°$.
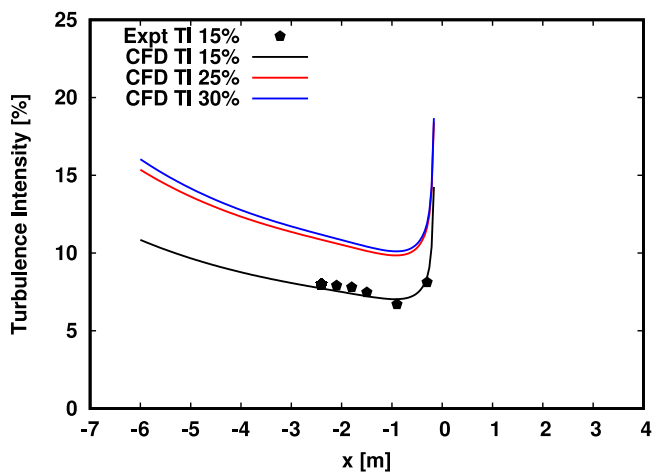

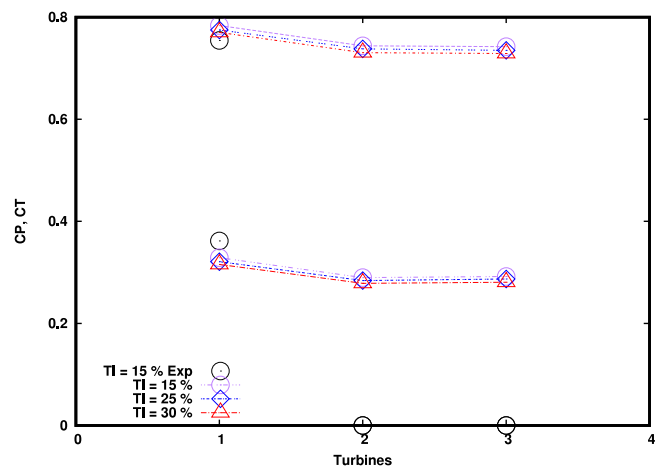**Fig. 8.** Turbulence intensities decay variation in the three array turbine, TSR = 7.

Fig. 9. Comparison of coefficient of power C_P (bottom) and coefficient of thrust C_T (bottom) at different upstream turbulence intensities, TSR = 7.
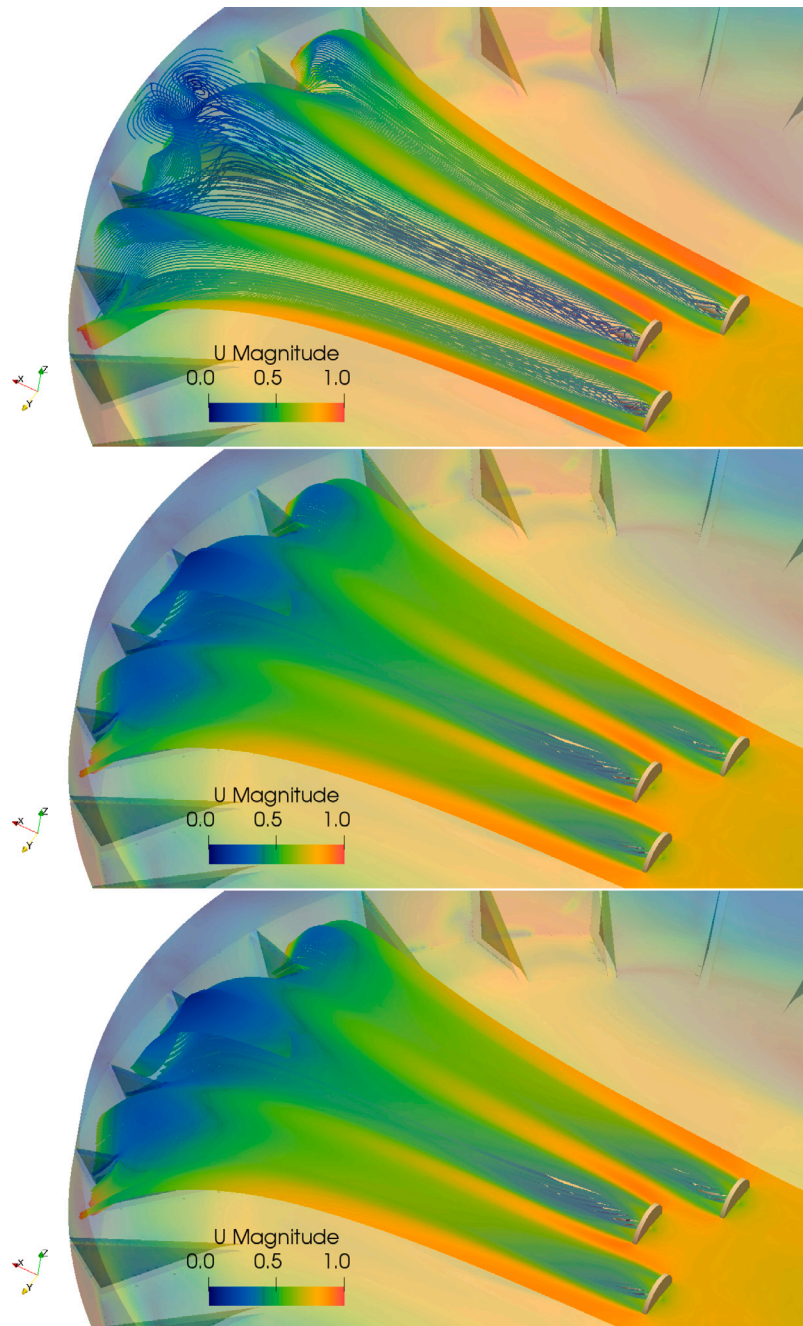
Fig. 10. Wake velocity for the three turbine array at different upstream turbulence intensities. Top to bottom: $TI = 15\%$, $TI = 25\%$, $TI = 30\%$.

width is 300 metres (y-axis). A uniform and steady velocity profile of 3.0 m/s, which is the nominal inflow velocity and turbulence intensities of 1%, 5% and 10% were applied at the inlet of the computation domain. This is applicable here as the turbine arrays are placed in a wide channel and therefore only extract a small fraction of the energy available to them. Future large-scale generation will undoubtedly require the deployment of hundreds of devices at high-energy locations. Such locations are fairly limited and hence, the devices are likely to be packed relatively closely to one another along the seabed. A high density of tidal turbines will cause excessive resistance to the flow, or in effect an increase in the drag coefficient of the channel, causing a reduction of flow velocities at the devices (Garrett and Cummins, 2005). Under such circumstances, a different turbine optimisation will be required than for a fixed upstream flow (Vennell, 2010, 2011).

Table 5
Simulation flow conditions.

Yaw, β (°)	$Turbulence\ intensity$, TI (%)
0	1
0	5
0	10
2	1
8	1

At the outlet boundary a zero gradient was applied. The nacelles and bottom of the domain are set to zero velocity and wall functions used for k, ϵ, and nut. No roughness parameter was added and the bottom boundary assumed a smooth wall. Five flow configurations, as illustrated in Table 5, were also carried out.
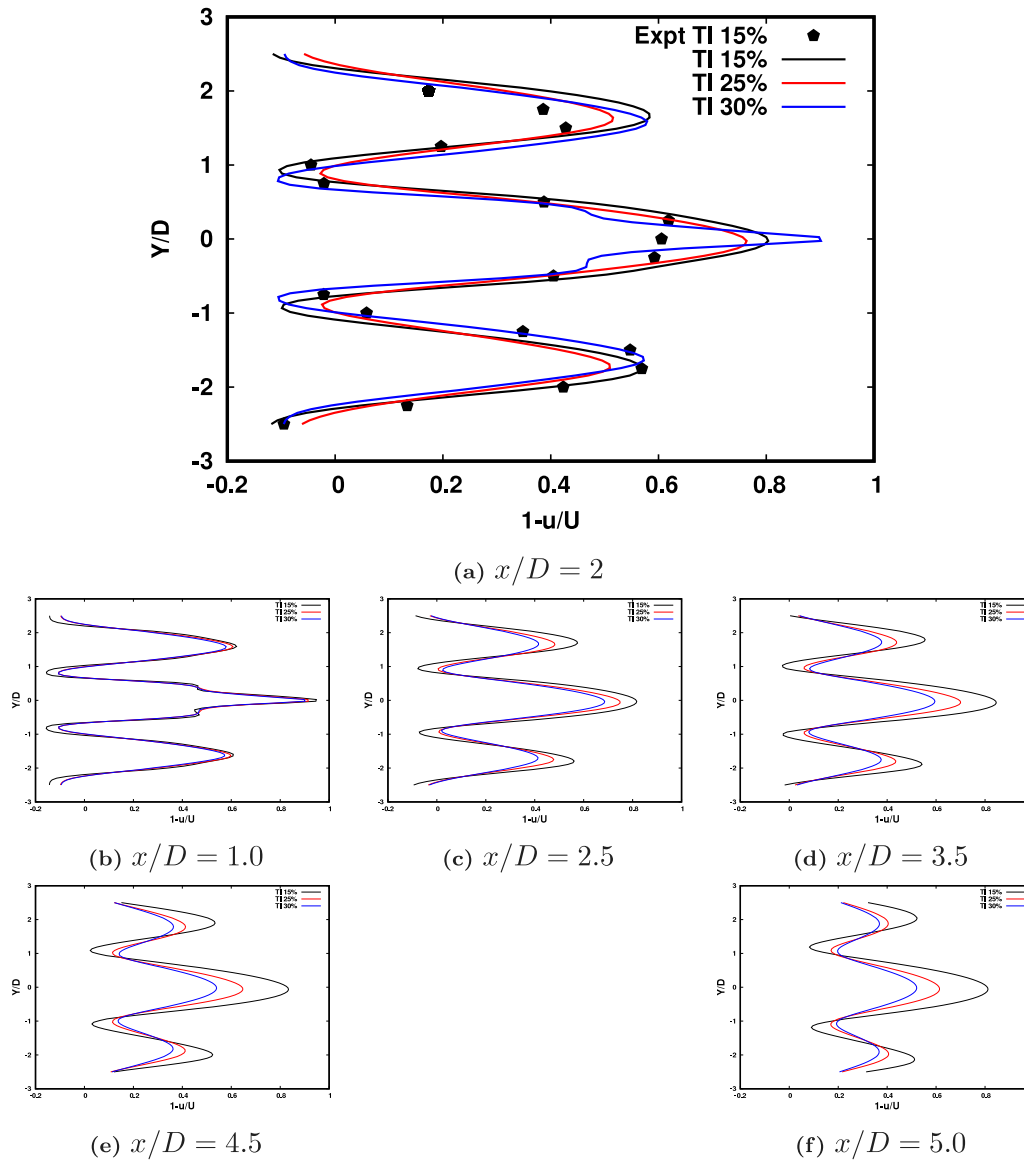
(a) $x/D = 2$

(b) $x/D = 1.0$

(c) $x/D = 2.5$

(d) $x/D = 3.5$

(e) $x/D = 4.5$

(f) $x/D = 5.0$

Fig. 11. Transverse profiles of normalised downstream axial velocities at three different upstream turbulence intensities.

4.3. Grid generation

All grids were created utilising both "blockMesh" and "snappyHexMesh" in OpenFOAM version 6.0. The "blockMesh" utility is used to generate an initial block (mesh domain) with size set to 1200 m × 300 m × 30 m in *x*, *y*, and *z* directions respectively which captures the domain extents. The discretisation does not use any grading in this case thus "simpleGrading" is set to one. Refinement of the mesh around the turbines and wake region is achieved using "snappyHexMesh" utility. The wake region is defined as a cylinder 37.5 metre radius, extending from the rotor to 900 metres downstream, i.e. to the domain outflow. The refinement level in this region is specified as level 2. The rotor assembly and bladebox is set with a refinement level of 4.

Mesh dependency of the simulations within the blade-box and wake regions was assessed in Malki et al. (2014) and Edmunds et al. (2017b) respectively with the turbine operating close to an optimal design TSR of 3.0. Based on the recommendations in these previous studies, subdivisions of 480 × 120 × 12 with total element size of approximately 25 M representing a reasonable compromise in accuracy and computational cost, was chosen to perform the remaining studies.

4.4. Results

4.4.1. Performance at different yaw angles

This section presents the performance of both regular and modified array configurations in straight flow conditions, with inlet turbulence defined by TI = 1%. The individual devices within the arrays and the hydrodynamic flow structures between the turbines are also evaluated. Figs. 14 and 15 present the coefficient of power, C_P, and thrust, C_T, for the two configurations at the different yaw angles. C_P and C_T were also calculated based on the inflow velocity and a fixed TSR. The computed power production at $\beta = 0°$ for the front four set of turbines in the modified formation was 1.826 MW. At $\beta = 2°$ and $8°$, the power production reduced to 1.767 MW and 1.733 MW respectively, about 3% and 5% less than the $\beta = 0°$ case. These values are significantly less than the 0.06% and 1.0% reduction in C_P that would be expected if yaw effects were only assumed to be a function of the decreased projected swept area of the turbine. Similar tendencies were observed in the regular formation.

There were however large differences in power in the second to fourth sets of turbines, more especially turbines 8–14. Starting with the modified formation at the higher yaw angle, turbines 8, 9 and 12 were
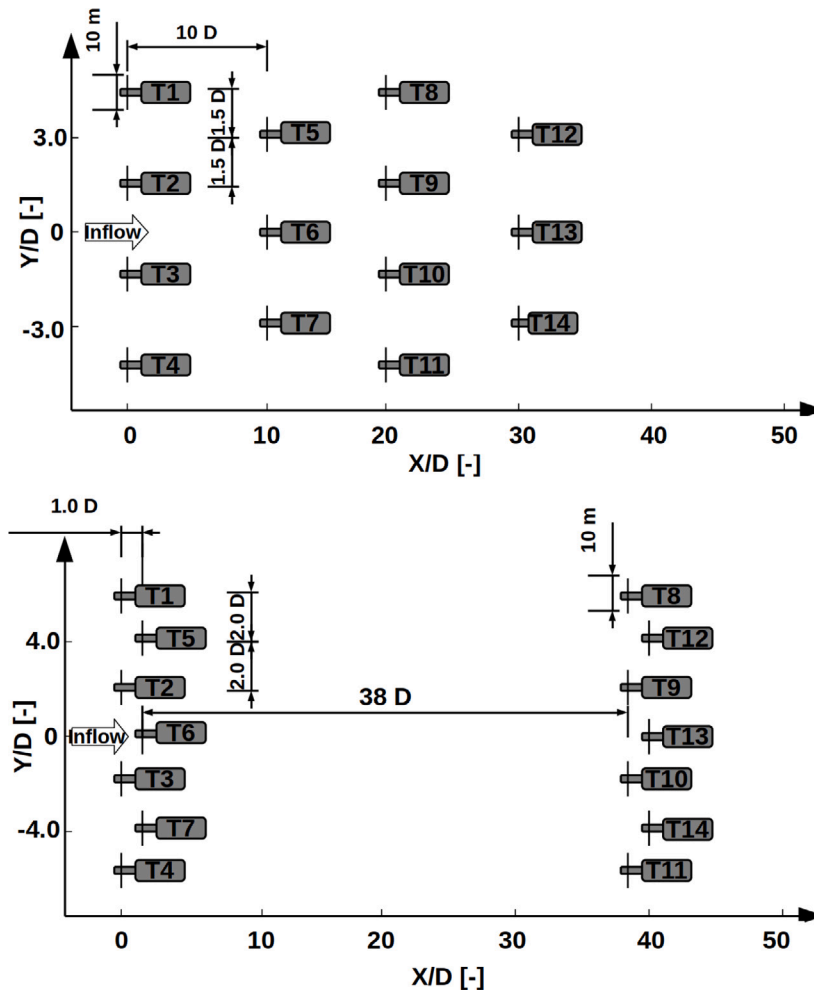
Fig. 12. Schematics of the 14-turbine layout: (top) regular formation (bottom) modified formation including rotor numbers (not to scale).
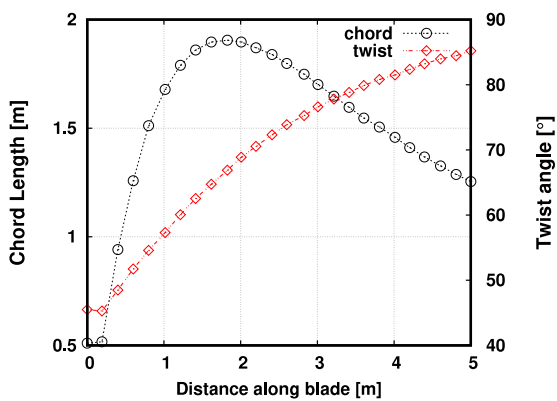

Fig. 13. Chord length and twist characteristics of the blades used in the 14-turbine layout analysis.

not directly affected by the wake of the front set of turbines (i.e turbines 1–7). The inflow to these turbines were almost similar to freestream conditions (see also Fig. 17). This resulted in an increase in their C_P values and a further increase in C_P for turbine 12 which also took advantage of the bypass flow. All the other turbines experienced some disturbances from the wake generated by turbines 1–7 and resulted in

reduced C_P values with a further decrease in C_P in turbines 10 and 11 due to the reduced wake recovery and the smaller recovery distance of the upstream turbines (5 and 6). In the $\beta = 2°$ case, all rear turbines with the exception of turbine 8 experienced disturbance from the wake generated by turbines 1–7. Table 6 shows the computed power for each row of turbines at $\beta = 0°$, 2° and 8°. From these values, it can be seen that apart from the third row of turbines, power production decreases with increase in yaw angle.

Similar tendencies were also found in the regular formation. The predicted overall farm power was 5.32 MW, 5.25 MW, 3.64 MW compared to 5.86 MW, 5.83 MW, 5.96 MW in the modified formation at $\beta = 0°$, 2° and 8° respectively. Although the overall farm power was higher in the modified formation compared to the regular formation for the investigated yaw cases, interestingly the highest power output was not necessarily obtained for the modified tidal farm at $\beta = 0°$, but for $\beta = 8°$ in this case. This shows that for larger tidal farms, the overall power output at yaw that can be obtained compared to the straight flow cases can either increase (or decrease) since the power output in rows further downstream depends on the orientation in the first rows. The results also show that strong sensitivity of tidal farm power output to small variations of the inflow direction exists and this should be taken into account for optimal control as well as grid integration of tidal farms. Similar tendencies were observed in the coefficient of thrust C_T values in Fig. 15 where C_T decreases as yaw angle increases due to the reduced axial component of the velocity rather than the spanwise component as thrust depends on the axial component.
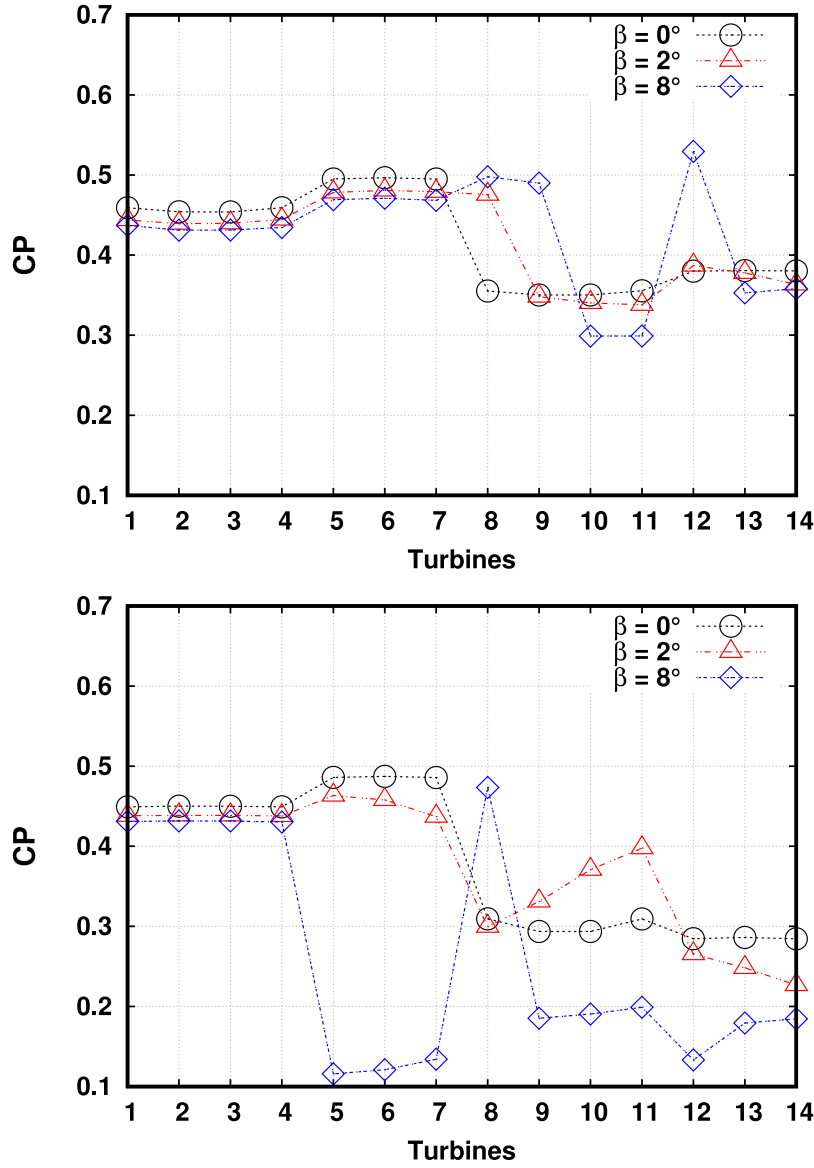
Fig. 14. Comparison of coefficient of power C_P for the modified (top) and regular (bottom) configuration at different yaw angles, TI = 1%, TSR = 3.

Table 6
Power for each row of turbines in the two layouts at different yaw angles, TI = 1%.

Configuration	Row No	$\beta = 0°$	$\beta = 2°$	$\beta = 8°$
Modified	1	1.826 MW	1.767 MW	1.733 MW
Modified	2	1.487 MW	1.438 MW	1.408 MW
Modified	3	1.411 MW	1.502 MW	1.585 MW
Modified	4	1.141 MW	1.128 MW	1.240 MW
Regular	1	1.798 MW	1.753 MW	1.724 MW
Regular	2	1.459 MW	1.358 MW	0.371 MW
Regular	3	1.206 MW	1.399 MW	1.048 MW
Regular	4	0.855 MW	0.740 MW	0.497 MW

Figs. 16 and 17 show the calculated wake velocities for the two configurations at the different yaw angles. The overall wake structure, wake width and expansion rates are similar for all three yaw angles. However, similar to the three turbine array, there is a slight increase in skewness in the wake and a decrease in the wake recovery distance at the highest yaw angle, seen more clearly in the Fig. 16.

4.4.2. Performance at different upstream turbulence intensities, $TI's$

Figs. 18 and 19 present the results for power and thrust coefficients for the two configurations at three different upstream turbulence intensities, $TI = 1\%$, 5% and 10% at $\beta = 0°$. Similar to the three turbine array, for the front set of turbines in both configurations, TI has little effect on the mean C_P and C_T for the $TI's$ evaluated in this analysis, with less than 3% difference. However, a closer inspection of the plots show some visible differences, especially in the rear sets of turbines, where it appears that increasing the turbulence intensity from 1% to 10% increases both C_P and C_T.

Table 7 shows the computed power production for the first to fourth rows of turbines for the modified formation at $TI = 1\%$, 5% and 10%. The results show an increase of 11% in power production when inlet TI is increased to 5% and a further increase of 0.5% in the power production when inlet TI is increased to 10% whilst in the regular formation, an increase of 4% in power production is observed when inlet TI is increased to 5% and a further increase of 7% when inlet TI is increased to 10%. Comparing both modified and regular formations, these values corresponds to a 10.26%, 19.75% and 11.08% increase in
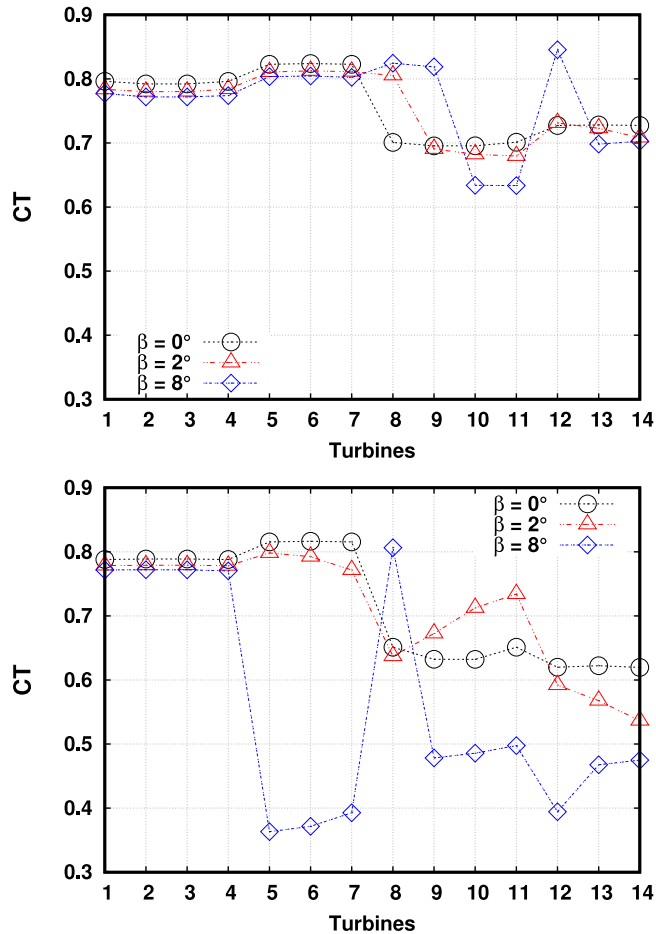
Fig. 15. Comparison of coefficient of thrust C_T for the modified (top) and regular (bottom) configuration at different yaw angles, TI = 1%, TSR = 3.

Table 7
Power for each row of turbines in the two layouts at different turbulence intensities.

Configuration	Row No	TI = 1%	TI = 5%	TI = 10%
Modified	1	1.826 MW	1.863 MW	1.883 MW
Modified	2	1.487 MW	1.511 MW	1.542 MW
Modified	3	1.411 MW	1.780 MW	1.789 MW
Modified	4	1.141 MW	1.438 MW	1.414 MW
Regular	1	1.798 MW	1.837 MW	1.859 MW
Regular	2	1.459 MW	1.477 MW	1.488 MW
Regular	3	1.206 MW	1.287 MW	1.544 MW
Regular	4	0.855 MW	0.904 MW	1.059 MW

5. Summary

This paper introduces modelling techniques for better understanding of the performance variations and wake effects of two different tidal stream array configurations. First, a three turbine array was modelled, followed by a fourteen turbine array with standard hypothetical staggered arrangement of four rows with constant lateral and longitudinal spacing of 3.0 and 10.0 diameters respectively. The array layout was then altered by moving the second and third rows so they are 1D from the first and fourth rows. A performance study was conducted by comparing the thrust and power coefficients under varying effects of yaw angles and upstream inflow turbulence. A summary of the important findings are outlined below:

5.1. Yawed flow

5.1.1. Three turbine array
- The performance characteristics for the straight flow in the three turbines array are in close agreement with previous studies (Noble et al., 2020).
- Power and thrust decreased as yaw was increased.
- Yaw was found to have minimal effect on the individual wakes, however small increase in skewness and decrease in recovery was found at the higher yaw angle compared to the straight flow case.
- Yaw resulted in a shift in the wake plots. However, the profile of the primary turbine show similar behaviour with the straight flow in the near wake. Interestingly, for the two upstream turbines, the plots also show that $\beta = 0°$ has the largest velocity deficit for turbine 3 whereas it has the smallest velocity deficit for turbine 2 in the near wake. It is possible that this might be a feature of the complex tank velocity rather than yaw.

5.1.2. Fourteen turbine array
- Compared to the regular staggered configuration at $\beta = 0°$, the total power output of the modified array was increased by over 10%. Wake recovery to freestream was also better in the modified formation compared to the regular staggered configuration.
- Lateral spacing between devices in straight flow conditions affected the rate of flow recovery downstream. It was shown that for lateral spacing of 4D there was faster downstream recovery compared to the 3D. This is relevant in the context of large arrays where further devices may be placed downstream.
- Similar to the three turbine array, power and thrust coefficient decrease with increase in yaw angle in the front set of turbines. However, the results are non-linear with the move away from optimal TSR in combination with reduced upstream U to the rear turbines.
- Depending on the yaw angle, most of the individual devices downstream were directly affected by the wakes of the upstream devices, resulting in reduced power and thrust. However, few of the devices experienced inflow conditions similar to the freestream resulting in power and thrust increases.
- Strong sensitivity of tidal-farm power exists even to small variations of inflow direction. This is relevant for optimal control as well as grid integration of tidal farms.
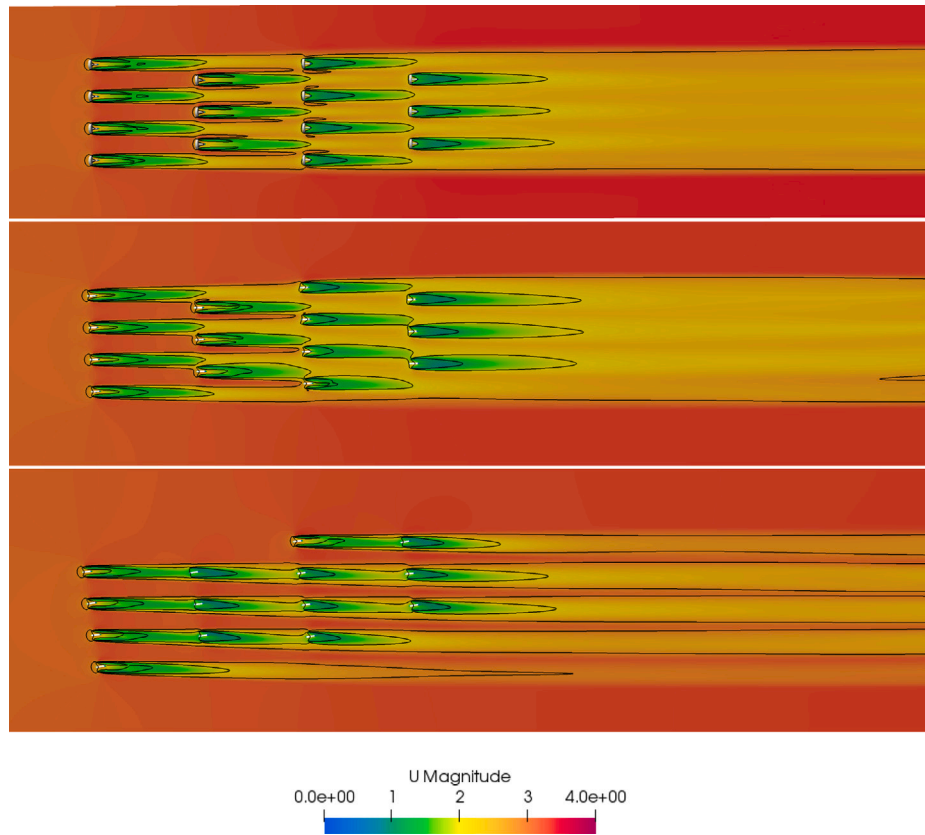
overall farm power in the modified formation for $TI = 1\%$, 5% and 10% respectively.

These results are very important especially as large arrays are likely to be deployed in staggered arrangements to maximise the performance of downstream devices and the model results presented here indicate that TI influences downstream devices. It is also likely that the force fluctuations, hence fatigue loads could also be affected, a factor that is relevant when optimising turbine designs to increase reliability. The relatively low values of TI used in the analysis will likely be found in strait channels without many features that will increase turbulence levels.

Figs. 20–21 show TI influence on the wake velocities for the two configurations. Again, it can be seen that TI plays a major role in the wake details. Both wake length and wake width increase with an increase in TI. Near wake features were similar but recovery was more quicker in the higher turbulence case. This is seen more clearly in Fig. 20 where the wake of the front set of turbines recovers quickly as it approaches the rear turbines in the higher turbulence case. Turbulence intensity helps to recover the axial velocity in the wake and the width of the wake increases with turbulence intensity in the far wake, meaning that the arrays will have a wider wake when operating in turbulent environments.

Fig. 16. Wake velocity for the regular formation at different yaw angles. Top to bottom: $\beta = 0°$, $2°$, $8°$, Isolines at 95% inlet velocity.
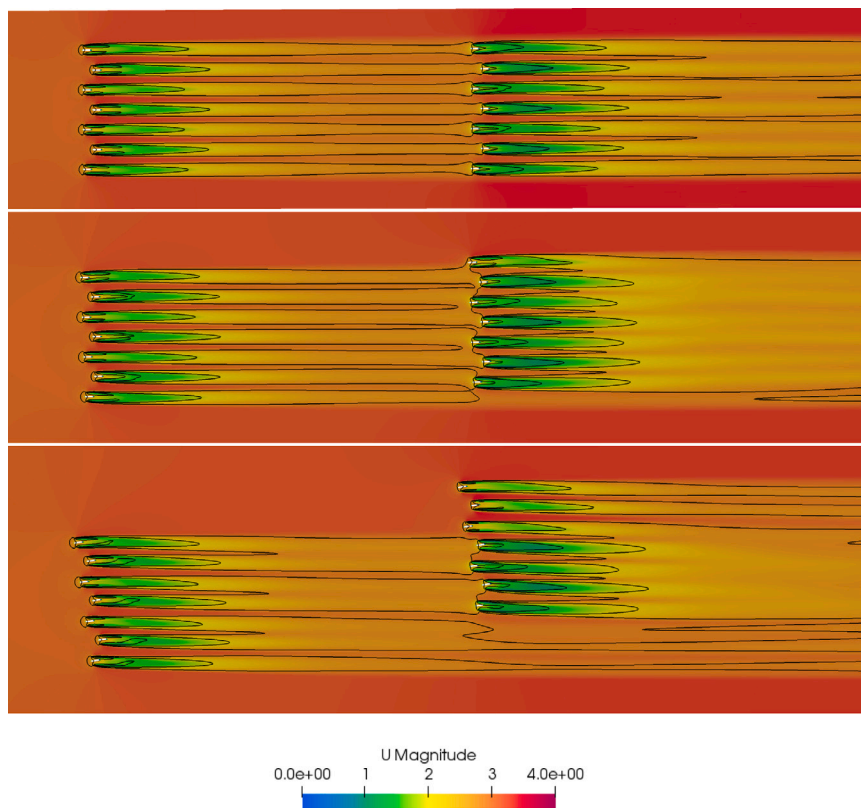

Fig. 17. Wake velocity for the modified formation at different yaw angles. Top to bottom: $\beta = 0°$, $2°$, $8°$, Isolines at 95% inlet velocity.
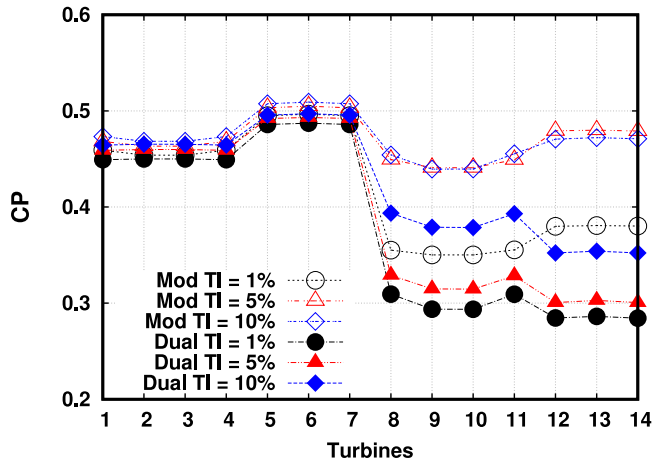
Fig. 18. Comparison of coefficient of power C_P for the modified (hollow points) and regular formation (solid points) at three different upstream turbulence intensities.
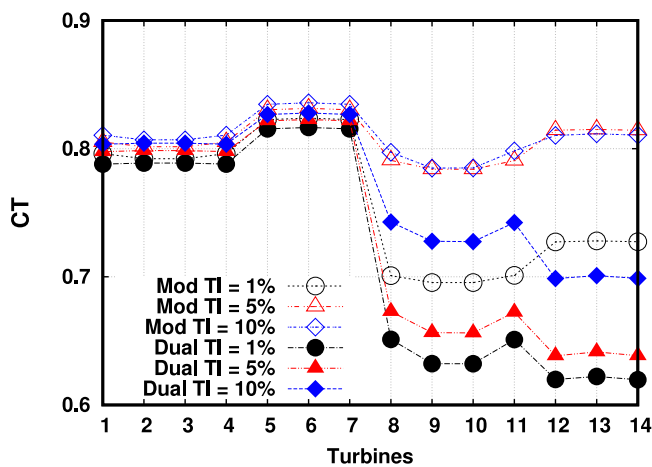

Fig. 19. Comparison of coefficient of thrust C_T for the modified (hollow points) and regular formation (solid points) at three different upstream turbulence intensities.

5.2. Upstream turbulence intensities: Three and fourteen turbine array

- Turbulence intensity was found to decay rapidly shortly downstream of the inlet which is consistent with experimental data.
- Turbulence intensity helps in recovery of axial velocity in the wake.
- Wake width increases with turbulence intensity in the far wake, meaning that arrays will have a wider wake when operating in turbulent environments.
- Turbulence intensity had little effect on the thrust and power of the front set of devices in the array. It is important to stress that each of these results have been obtained using a fixed TSR and a time averaged representation of the flow. It is likely that using the local TSR's at the turbines as well as a transient model could influence the results.

6. Conclusions and future work

In conclusion, an efficient method for simulating tidal stream energy converter rotor response to realistic inflow and turbulence intensity

conditions and capturing the subsequent impact to farfield flow structure using a GAD-CFD approach has been demonstrated. Model validation against experimental testing has been conducted and the results show that large array layouts influence on the flow around a downstream device is complex both in straight and yawed flow and would be difficult to characterise using simple empirical relationship. The results could help understand/improve array configurations. Further validation of the model would be recommended as more experimental data becomes available and the model improved to account for more complex flow details. However, the study provides confidence that the approach can be applied to a range of scenarios; both laboratory scale, and large scale deployments in both the marine and wind environments.

Due to the computational efficiency, such an approach, especially when compared to fully resolved turbine geometry models, makes the GAD-CFD technique suitable for modelling arrays consisting of a large number of rotors and for conducting multiple model runs under varying tidal and machine-operating-point conditions. It is therefore appropriate to also consider the model for studying tidal stream arrays and their interaction with respect to local topography and power control.

Since tidal energy could play an important role in decarbonising electricity generation it is important to have access to efficient and accurate engineering tools such as the one developed here (which sits between highly detailed blade resolved models and larger scale oceanographic and atmospheric models). Improved modelling will reduce the technical risk of operating these devices in the highly energetic marine environment thus increasing economic viability of the sector.

Future work should focus on improving the model to account for changing lift and drag characteristics at higher levels of free stream turbulence. As turbulence levels increase, the quantity of lift and drag changes, as does the stall point relative to angle of attack, and post stall features significantly change. The model could also be combined with turbine control algorithms that consider power capping through stall or pitch control to enable the study of rotors. Other factors that will also affect device performance in natural environments such as bathymetric effects and bottom roughness need to be included as this will assist in improving existing methods for performance prediction.

Beyond this immediate application the developers seek to develop and incorporate more realistic bathymetry characterisations, which is expected to be an important factor in real-world turbine array operation. It is the authors intention to publish the implementation of the model to enable such studies to take place.

Declaration of competing interest

The authors declare that they have no known competing financial interests or personal relationships that could have appeared to influence the work reported in this paper.

Data availability

Data will be made available on request.
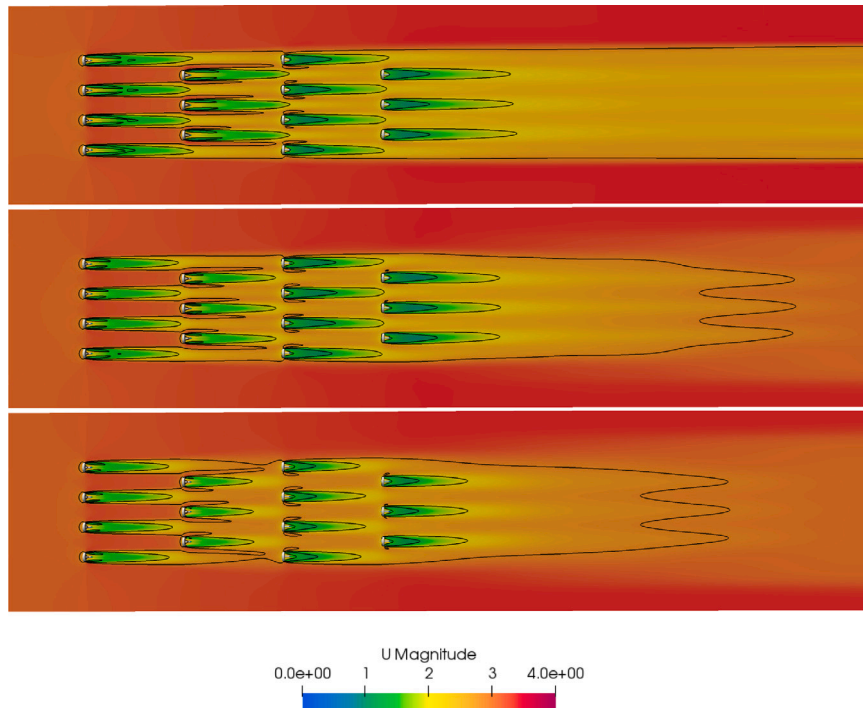
Acknowledgement

Fig. 20. Wake velocity for the regular formation at three different upstream turbulence intensities. Top to bottom: TI = 1%, 5%, 10%, Isolines at 95% inlet velocity.
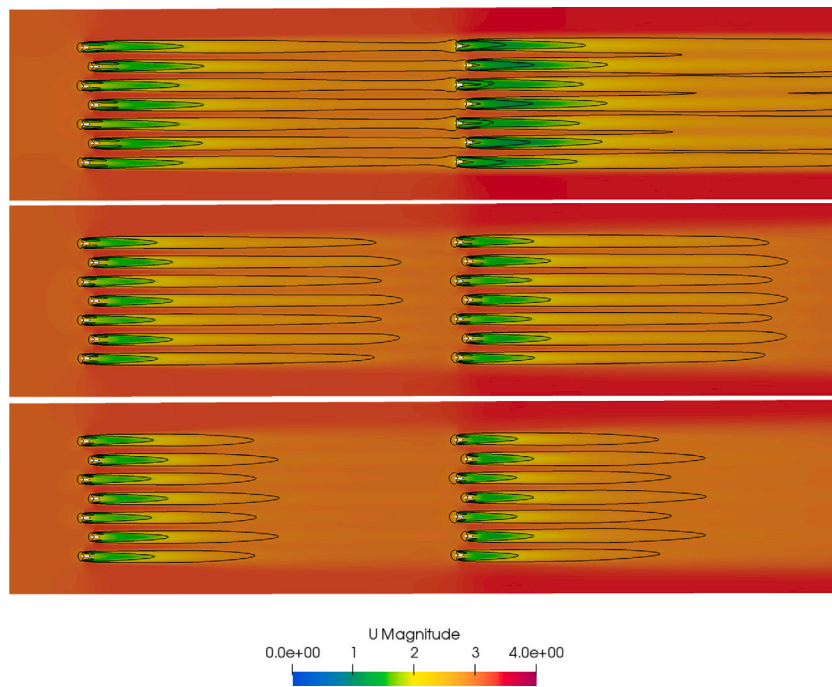

Fig. 21. Wake velocity for the modified formation at three different upstream turbulence intensities. Top to bottom: TI = 1%, 5%, 10%, Isolines at 95% inlet velocity.

References

Abbott, I., Von Doenhoff, A., 1959. Theory of Wing Sections, Including a Summary of Airfoil Data. In: No. 1 in Dover Books on Aeronautical Engineering Series.

Adaramola, M., Krogstad, P., 2011. Experimental investigation of wake effects on wind turbine performance. Renew. Energy 36, 2078–2086.

Badoe, C., Edmunds, M., Nambiar, A., Williams, A., Sellar, B., Kiprakis, A., Masters, I., 2022a. Robust validation of a generalised actuator disk CFD model for tidal turbine analysis using the FloWave ocean energy research facility. Renew. Energy 190, 232–250.

Badoe, C., Li, X., Armstrong, S., Williams, A., Masters, I., 2021. Tidal stream turbine arrays in a demonstration site using GAD-cfd models. In: Proc of the 9th Conf on Comp Methods in Marine Eng (Marine 2021).

Badoe, C., Li, X., Williams, A., Masters, I., 2022b. Computational fluid dynamics modelling of tidal turbine arrays in a demonstration site. In: Proc of the Int Conf on Renewable Energies Offshore (RENEW 2022).

Bahaj, A., Molland, A., Chaplin, J., Batten, W., 2007. Power and thrust measurements of marine current turbines under various hydrodynamic flow conditions in a cavitation tunnel and a towing tank. Renew. Energy 32, 407–426.

Bahaj, A., Molland, A., Chaplin, J., Batten, W., 2013. Marine current energy conversion: the dawn of a new era in electricity production. Philos. Trans. A Math. Phys. Eng. Sci. 371, 20120500.

Baratchi, R., Jeans, T.L., Gerber, A.G., 2017. Actuator line simulation of a tidal turbine in straight and yawed flows. Int. J. Mar. Eng. 19, 235–255.

Batten, W.M.J., Harrison, M.E., Bahaj, A.S., 2013. Accuracy of the actuator disc-RANS approach for predicting the performance and wake of tidal turbines. Philos. Trans. R. Soc. Lond. Ser. A: Maths. Phys. Eng. Sci..

Ebdon, T., O'Doherty, T., Mason-Jones, A., O'Doherty, D.M., 2016. Simulating marine current turbine wakes with advanced turbulence models. In: Proc of the 3rd Asian Wave and Tidal Energy Conference.

Edmunds, M., Masters, I., Banerjee, A., Williams, A., VanZwieten, J.H., 2020. A spatially nonlinear generalised actuator disk model for the simulation of horizontal axis wind and tidal turbines. Energy 194.

Edmunds, M., Williams, A., Masters, I., 2017a. Power shedding from stall and pitch controlled tidal stream turbines. In: Proc of 11th Euro Wave and Tidal Eng Conf.

Edmunds, M., Williams, A., Masters, I., Croft, T.N., 2017b. An enhanced disk averaged CFD model for the simulation of horizontal axis tidal turbines. Renew. Energy 101, 67–81.

Galloway, P.W., Myers, L.E., Bahaj, A.S., 2011. Experimental and numerical results of rotor power and thrust of a tidal turbine operating at yaw and in waves. In: World Renewable Energy Congress. Linkoping, Sweden, pp. 8–13.

Galloway, P.W., Myers, L.E., Bahaj, A.S., 2014. Quantifying wave and yaw effects on a scale tidal stream turbine. Renew. Energy 63, 297–307.

Gao, Z., Li, Y., Tongguang, W., Wenzhong, S., Xiaobo, Z., Pröbsting, S., Li, D., Li, R., 2021. Modelling the nacelle wake of a horizontal-axis wind turbine under different yaw conditions. Renew. Energyy 172, 263–275.

Garrett, C., Cummins, P., 2005. The power potential of tidal currents in channels. Proc. R. Soc. Lond. Ser. A Math. Phys. Eng. Sci. 461, 2563–2572.

Howland, M., Bossuyt, J., Tossas, M., Meyers, J., Meneveau, C., 2016. Wake structure in actuator disk models of wind turbines in yaw under uniform inflow conditions. J. Renew. Sustain. Energy 8.

Maganga, F., Germain, G., King, K., Pinon, G., Rivoalen, E., 2009. Experimental study to determine flow characteristic effects on marine current turbine behaviour. In: Proc of the Euro Wave and Tidal Energy Conf.

Malki, R., Masters, I., Williams, A., Croft, T.N., 2014. Planning tidal stream turbine array layouts using a coupled blade element momentum–computational fluid dynamics model. Renew. Energy 63, 46–54.

Malki, R., Williams, A., Masters, I., Togneri, M., Croft, T.N., 2013. A coupled blade element momentum-computational fluid dynamics model for evaluating tidal stream turbine performance. Appl. Math. Model. 37, 3006–3020.

McNaughton, J., Rolfo, S., Apsley, D., Afgan, I., Stallad, T., Stansby, P., 2013. Turbulent flow and loading on a tidal stream turbine by LES and RANS. Int. J. Heat Fluid Flow. 75, 96–108.

Modali, P., Kolekar, N.S., Banerjee, A., 2018. Performance and wake characteristics of a tidal turbine under yaw. Int. J. Mar. Eng. 1, 41–50.

Noble, D., Davey, T., Smith, H.C.M., Kaklis, P., Robinson, A., Bruce, T., 2015. Characterisation of spatial variation in currents generated in the FloWave ocean energy research facility. In: Proc of 11th Euro Wave and Tidal Eng Conf.

Noble, D., Draycott, S., Nambiar, A., Sellar, B., Steynor, B., Kiprakis, A., 2020. Experimental assessment of flow, performance, and loads for tidal turbines in a closely-spaced array. Energies.

O'Doherty, T., Mason-Jones, A., O'Doherty, D.M., Byrne, C., Owen, I., Wang, Y.X., 2009a. Experimental and computational analysis of a model horizontal axis tidal turbine. In: Proc of the Euro Wave and Tidal Energy Conf.

O'Doherty, D., Mason-Jones, A., O'Doherty, T., Byrne, C., Owen, I., Wang, W., 2009b. Considerations of improved tidal stream turbine performance using double rows of contra-rotating blades. In: Proc of the Euro Wave and Tidal Energy Conf.

Olczak, A., Stallard, T., Feng, T., Stansby, T., 2014. Comparison of a RANS blade element model for tidal turbine arrays with laboratory scale measurements of wake velocity and rotor thrust. J. Fluids Struct. 64, 87–106.

Payne, G.S., Stallard, T., Martinez, R., 2017. Design and manufacture of a bed supported tidal turbine model for blade and shaft load measurement in turbulent flow and waves. Renew. Energy 107, 312–326.

Piano, M., Neill, S.P., Lewis, M.J., Robins, P.E., Hashemi, M.R., Davies, A.G., Ward, S.L., Roberts, M.J., 2017. Tidal stream resource assessment uncertainty due to flow asymmetry and turbine yaw misalignment. Energy 114, 1363–1375.

Schulz, C., Letzgus, P., Lutz, T., Kramer, E., 2017. CFD study on the impact of yawed inflow on loads, power and near wake of a generic wind turbine. Wind Energy 20, 253–268.

Sutherland, D.R.J., Noble, D., Davey, T., Steynor, J., Davey, T.A.D., Bruce, T., 2017. Characterisation of current and turbulence in the FloWave ocean energy research facility. Ocean Eng. 139, 103–115.

The Crown Estate, 2018. UK wave and tidal Key Resource Areas project. Tech. Rep., Version 2. http://www.thecrownestate.co.uk/, Retrieved: 2018.

Tian, W., VanZwieten, J., Pyakurel, P., Li, Y., 2016. Influences of yaw angle and turbulence intensity on the performance of a 20 kW in-stream hydrokinetic turbine. Energy 111, 104–116.

Tongchitpakdee, C., Benjanirat, S., Sankar, L., 2005. Numerical simulation of the aerodynamics of horizontal axis wind turbines under yawed flow conditions. J. Sol. Energy Eng. 127, 464–474.

Turnock, S., Phillips, A., Nicholls-Lee, R., 2011. Modelling tidal current turbine wakes using a coupled RANS-BEMT approach as a tool for analysing power capture of arrays of turbines. Ocean Eng. 38, 1300–1307.

Vennell, R., 2010. Tuning turbines in a tidal channel. J. Fluid Mech. 663, 253–267.

Vennell, R., 2011. Tuning tidal turbines in-concert to maximise farm efficiency. J. Fluid Mech. 671, 587–604.

Weller, H.G., Tabor, G., Jasak, H., Fureby, C., 1998. A tensorial approach to computational continuum mechanics using object-oriented techniques. J. Comput. Phys. 12, 620–631.

Zhang, C., Zhang, J., Angeloudis, A., Zhou, Y., Kramer, S., Piggott, M., 2023. Physical modelling of tidal stream turbine wake structures under yaw conditions. Energies 16, 1742.